New functionalities of a bone cement by adding mechanochemically synthesized magnetic nanoparticles.

Pedro A. Calderón Bedoya[a*], Pablo M. Botta[a], María V. Álvarez[b], Paula G. Bercoff[c], Enio Lima[d], Roberto Zysler[d], María A. Fanovich[a]

[a]*Institute of Materials Science and Technology (INTEMA), University of Mar del Plata and National Research Council (CONICET), Av. Colón 10850, Mar del Plata, Argentina.*

[b]*Grupo de Investigación en Ingeniería en Alimentos. Instituto de Ciencia y Tecnología de Alimentos y Ambiente (INCITAA), Facultad de Ingeniería. Universidad Nacional de Mar del Plata. Mar del Plata, Argentina.*
[c]*Instituto de Física Enrique Gaviola (IFEG), CONICET-UNC, Medina Allende s/n, Córdoba, Argentina.*
[d]*Laboratorio de Resonancias Magnéticas, CAB-CNEA, S.C. de Bariloche, Argentina.*

ABSTRACT

New formulations of calcium phosphate cements (CPCs) with magnetic properties have been developed. The CPC matrix was prepared from an equimolar mixture of tetracalcium phosphate (TTCP) and anhydrous calcium hydrogen phosphate (DCPA), using Na_2HPO_4 solution as liquid phase. Naked and functionalized iron oxides nanoparticles (IONPs), were incorporated into the CPC solid phase and the effect of the different contents of IONPs on the initial and final setting times of the CPCs was investigated. Moreover, magnetic properties, antibacterial activity and magnetic hyperthermia response of these systems were evaluated. The results showed a clear influence of the IONPs in the setting process, with low conversion of hydroxyapatite (HA), especially for contents greater than 10 wt%. Magnetization values of 5.6 and 11.4 emu/g at the maximum applied field (13 kOe) for CPC with 10 and 20 wt% of IONPs respectively, were obtained. Magnetic hyperthermia of CPC with 10 wt% of IONPs showed a specific power absorption (SPA) of 0.22 (W/g). Similar values of SPA were obtained for cements with functionalized IONPs. Also, CPC with 10 wt% of functionalized IONPs with usnic acid showed antibacterial activity against *L. inoccua.* These data are promising, considering that the concentration of IONPs in the cement is only equivalent to 10 wt% of the material.

KEYWORDS

A. Powders: chemical preparation; C. Magnetic properties; E. Biomedical applications.

1. INTRODUCTION

Calcium phosphate cements (CPCs) are widely used as bone replacement materials showing excellent bioactivity, because they closely resemble natural bone in structure and composition. CPCs have attracted increased attention as biomaterials because of their injectability and in situ self-setting properties, which allow for minimally invasive surgical procedures and local drug delivery. Different mixtures of calcium phosphates have been studied as bone cements, among them the most successful composition, from a physicochemical point of view, is the tetracalcium phosphate (TTCP) and dicalcium phosphate anhydre (DCPA) mixture [1,2]. The setting reaction of these compounds, which originate by mixing the solid mixture with an aqueous phase, generates hydroxyapatite (HA) with a crystalline structure similar to that of human bones. CPCs have the advantage of optimal bone-defect filling capacity, and they are applicable through minimally-invasive surgery. The performance of such materials can be enhanced by incorporating active agents, or new functionalities [3–6].

On the other hand, magnetic hyperthermia (MH) presents a promising non-invasive approach to cancer therapy. It concerns the selective administration of magnetic nanoparticles to the tumor site, acting as a device for heat, followed by exposure to an external alternating magnetic field (AMF). Consequently, the tumor's temperature rises as a result of heat generation from the internalized magnetic nanoparticles under high-frequency AMF. This increase in temperature induces magnetic energy dissipation in single-domain particles, driven by both internal Néel fluctuations of the nanoparticle magnetic moment and external Brownian fluctuations. The elevated temperature effectively eradicates cancer cells through a variety of direct mechanisms and indirect response through the activation of the immune system [7].

Pylostomou *et al.* [8] recently reported a review that condenses the latest advances on CPC composite systems for the treatment of diseases such as osteoporosis, osteoarthritis, osteomyelitis, and other musculoskeletal disorders. Hyperthermia treatments with magnetic bone cements can not only treat deep bone tumor in a highly specifically way, but are also capable of achieving repair of weakened bone tissue. Also, there are reports on the development of magnetic CPC systems that are capable of controlling the hyperthermia temperature by themselves [9].

Xia *et al.* studied the *in vitro* and *in vivo* behavior of bone cements based on TTCP, DCPA and iron oxide magnetic nanoparticles (IONPs). These authors investigate the effects of magnetic nanoparticles as a liquid or powder on stem cells using IONPs-CPC prepared by adding 1% IONPs as liquid or powder. The study showed that it is highly promising to incorporate IONPs in CPC to enhance stem cell performance and bone regeneration efficacy. Incorporating IONPs as a liquid or as a powder into CPC both substantially enhanced adhesion, osteogenic differentiation, and bone mineral synthesis [10]. However, the magnetic hyperthermia response was not studied in this report, which is, the most attractive property of these materials for treating osteosarcoma.

Magnetic CPCs based on monetite ($CaHPO_4$) have also been prepared with the addition of magnetite particles in the composition. Ruskin *et al.* studied CPCs with variable amounts of magnetite (between 10% and 50%) with the objective of evaluating the cement's physicochemical characteristics as well as its biological behavior. These authors corroborated the possibility of generating heat by incorporating an optimized magnetite content (20%) in the temperature range of 40-45 °C due to power absorption from an applied alternating magnetic field. Furthermore, the compositions were bioactive and cytocompatible with an osteoblastic cell line [11].

The magnetic hyperthermia exhibited by magnetite or maghemite nanoparticles depends on the surrounding matrix. In a calcium phosphate cement, this environment is created during the setting of the cement paste through hydrolysis and precipitation, resulting that different cement formulations affecting the hyperthermia response. To our knowledge, there are no studies that show magnetic cements functionalized with IONPs obtained by mechanochemical methods. In this work, we study the effect of variable content of mechanosyntesized IONPs on the setting behavior of bone cements based on the TTCP and DCPA system. The magnetic nanoparticles were obtained through a method previously developed by our group, composed of maghemite/magnetite having magnetizations of the order of 65 emu/g and mean particle sizes of 9 nm [12]. Furthermore, the functionalization of CPC with IONPs containing usnic acid (as antibacterial agent) retained in a siloxane network obtained by sol-gel reaction in a supercritical CO_2 medium, was also evaluated.

2. MATERIALS AND METHODS

2.1 Synthesis of IONPs

Ferric chloride hexahydrate ($FeCl_3.6H_2O$, Biopack), Fe powder (Carlo Erba, particle size ~ 1 μm) and sodium hydroxide (NaOH, Anedra) were used as precursors for the synthesis of IONPs. All the chemicals used in the experiments were reagents of analytical grade and they were used without further purification. The precursor mixture was prepared by mixing solid reactants $FeCl_3.6H_2O$, Fe^0 and NaOH in a molar ratio of 8:1:24. The mixture (~10 g) was mechanochemically treated in a planetary ball mill (Fritsch Pulverisette 7), at 1400 rpm during 12 h. Zirconia balls (diameter 10 mm) and vials (25 mL) were used as milling materials. Mechanochemical treatment was performed at environmental conditions by using a milling-media/powder-mixture mass ratio of 6.4. The obtained powder was washed with distilled water to eliminate NaCl byproduct; after that, it was dried during 24 h at 50 °C [12,13].

2.2 Functionalization of IONPs

A mixture of 0.5 g of the synthesized IONPs with 0.85 g of 3-glycidyloxypropyltrimethoxysilane (Glymo) and 0.05 g of usnic acid (UA) was placed inside a high-pressure cell (Eurotechnica GmbH) and filled with CO_2 at 60 bar. Then, the temperature was raised to 40 ºC and the CO_2 pressure was increased up to 300 bars, conditions to generate supercritical CO_2. The system was maintained in these conditions for 2 h. Finally, the sample was washed with $scCO_2$ during 15 min with a flow rate of 2.3 L/min. Different preparations of IONPs functionalized (f-IONPs I, II, III and IV) with usnic acid retained in a siloxane network were obtained.

2.3 Preparation of calcium phosphate cement (CPC) with IONPs

The CPCs investigated in this study are composed of tetracalcium phosphate ($Ca_4(PO_4)_2O$, TTCP) and anhydrous calcium hydrogen phosphate ($CaHPO_4$, DCPA). TTCP was synthesized in our laboratory as reported elsewhere [14], from calcium carbonate, $CaCO_3$ (Merck) and diammonium hydrogen phosphate, $(NH_4)_2HPO_4$ (Merck).TTCP, commercial DCPA (Aldrich) and the synthesized IONPs were mixed to form the solid phase of CPC, using a mass ratio TTCP/DCPA of 2.69. A 5 % wt/V aqueous solution of Na_2HPO_4 (Aldrich) was used as liquid phase of the CPC (setting accelerator). All precursor reagents were analytical grade without further purification. The solid phase of CPC was mixed with Na_2HPO_4 solution until a homogeneous paste was obtained. The CPC compositions were prepared with 0, 5, 10, 20 and 30 wt % IONPs with respect to the solid phase mass, originating different samples named C, C5, C10, C20 and C30, respectively. Also, a CPC with 10 wt% of functionalized IONPs was prepared by the same method (sample C10GAU).

2.4 Characterization Methods

Identification of the crystalline phases of the synthesized IONPs and CPC samples was carried out by X-ray diffraction (XRD) in a PANalytical diffractometer with Cu-Kα radiation (λ = 1.54050 Å) at 40 kV and 30 mA. Diffractograms were recorded in a 2θ range between 20º and 40º at a scan rate of 1º/min. The mean crystallite size of IONPs was estimated from the XRD line broadening measurement, using the Scherrer equation [15] for the main peaks, considering the instrumental line width.

The particle size distributions of the IONPs were determined by dynamic light scattering (DLS) using a Malvern Zetasizer nano S90 with a 532 nm laser. Powders were dispersed in distilled water (5 mg in 10 mL) and sonicated for 10 min before each measurement.

Thermogravimetric analyses of functionalized IONPs were performed using a Shimadzu TG-50 instrument. Samples were heated up to 1000ºC at a heating rate of 5ºC/min in synthetic air flow.

Transmission electron microscopy (TEM) images of the IONPs and CPCs were obtained in a JEOL (JEM-2100) microscope with a voltage of 120 kV. Prior to observation, the samples were suspended in Cu grids after sonicating an isopropanol suspension of the IONPs for several minutes. Average particle size were obtained from TEM images, counting more than 200 elements with the Image Pro Plus software.

The setting time of the cements was measured according to the Gillmore needle method [ASTM C226-89]. The initial setting occurred when the light needle (mass of 113.4 g and diameter of 2.13 mm) failed to indent the surface of the sample, while the final setting time was determined by using the heavy needle (mass of 453.6 g and diameter of 1.06 mm). Each measurement was performed three times and the average value was calculated.

The morphologies of the consolidated CPCs were evaluated utilizing scanning electron microscopy

(SEM) in a Jeol JSM-6460 LV microscope equipped with energy dispersive X-ray spectroscopy (EDS). Prior to the observation the samples were sputtered with gold.

Magnetization (M) as a function of magnetic field (H) was measured in a vibrating sample magnetometer Lakeshore 7300 (VSM measurements). Hysteresis loops were registered at room temperature applying magnetic fields between - 13 kOe and + 13 kOe. Before performing the measurements, the IONPs powders were compacted in 0.5 mm thick pellets of 5 mm diameter**.**

Magnetic hyperthermia measurements were carried out in a D5-F1 device from NanoScale Biomagnetics, which consists of an RLC resonant circuit that works with two 70 nF capacitors and a water-cooled copper coil with 8 turns. To obtain the temperature curves as a function of time, the sample, in the form of a tablet, was placed in a Teflon sample holder that allows semi-adiabatic isolation of the system. The temperature was measured with a fiber optic sensor in physical contact with the sample. The working frequency of the applied alternating magnetic field was 413 kHz and the amplitude was 200 Oe. Respective cooling curves collected after the applied field was turned off were also acquired in order to allow estimation of the heat losses due to the non adiabaticity of the system.

In vitro antibacterial activities of the IONPs, IOPNPs-GAU and C, C10, C10GAU setting cements were evaluated by the agar diffusion method. Different indicator bacterial strains were used such as *Listeria innocua* CIP 80.11, *Staphylococcus aureus* ATCC 25923, *Escherichia coli* ATCC 36218 and *Pseudomonas aeruginosa* ATCC 15692. *L. innocua*, a non-pathogenic species, can be used as a biological indicator of the food pathogen *Listeria monocytogenes* due to its similar susceptibility to physical, chemical and thermal treatments. The stock cultures were maintained at 4 ºC. A 0.1 mL aliquot of each culture was added to 9.9 mL of Luria Bertani (LB) broth at two consecutive 24 h intervals followed by incubation at 37 ºC before each assay. For the assay, Müeller-Hinton agar plates were spread with 0.1 mL of the freshly grown culture (approx. 10^8 CFU/mL). Afterwards, 6 mm diameter wells were made on the agar plates, in which 20 µL of different suspensions of the powder extracts previously solubilized in dimethyl sulfoxide (DMSO) at a concentration of 60 mg/mL were placed. The plates were incubated at 37 ºC for 24-48 h, and then the growth inhibition zones were determined with a caliper. DMSO solvent was used as a negative control. The assays were performed in triplicate. The sensitivity of the indicator microorganisms to the different extracts can be classified according to the diameter of the inhibition zones as: not sensitive for diameters less than 8 mm; sensitive for diameters between 9-14 mm; very sensitive for diameters between 15-19 mm; and extremely sensitive for diameters greater than or equal to 20 mm [16].

Hardness and reduced Young's modulus (Er) were measured on both C and C10GAU samples using instrumented nanoindentation techniques. Mechanical testing was conducted with a Hysitron Triboindenter, equipped with a Berkovich nanoindenter tip and an MNRP system, applying forces ranging from 10 to 2500 mN. Based on preliminary trials, a force of 600 mN was selected to ensure minimum indentation depths of 15 µm in the materials.

3. RESULTS AND DISCUSSION

Firstly, the starting powders (TTCP, DCPA, and IONPs) were characterized by XRD. All the diffraction peak positions (Figure 1) match well with the reported XRD patterns of TTCP (PDF 25-1137), DCPA (PDF 77-0128), and IONPs (PDF 19-0629 and 39-1346 for magnetite and maghemite, respectively).

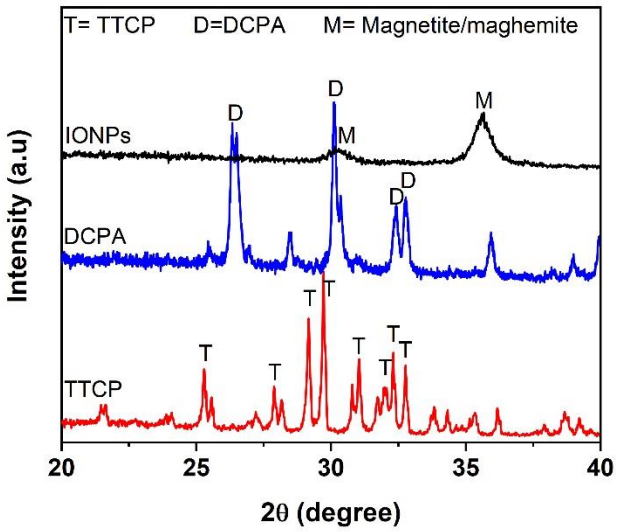

Figure 1: *XRD patterns of the starting powders for the preparation of the CPCs.*

Then, initial and final setting times (t_i and t_f) for CPC compositions with different IONPs content, by using Gillmore method were evaluated (Table 1). There are no significant variations in the t_i for samples C, C5 and

C10; the initial setting time was found to be ~5-6 min regardless the IONPs content. In contrast, C20 and C30 showed higher values of the initial setting time, reaching 22 min for C30. In all samples with different IONPs contents, the initial time is longer than in cements without IONPs. On the other hand, the final setting time for these samples showed a significant decrease compared to the CPC without nanoparticles, except for samples C20 and C30, (Table 1).

Table 1: *Powder to liquid ratio (P/L), initial (t_i) and final (t_f) setting times for each CPC composition.*

Sample	wt % IONPs	P/L	Setting time (min)	
			t_i	t_f
C	0	3.3±0.4	4.3±0.6	38.0±2.0
C5	5	4.3±0.1	6.0±1.3	26.0±2.5
C10	10	3.7±0.3	5.0±0.1	31.0±5.3
C10GAU	10	3.1±0.2	6.0±0.8	25.0±2.4
C20	20	3.3±0.2	9.6±2.5	41.0±5.7
C30	30	3.1±0.1	22.0±2.0	55.0±5.4

These values show a clear influence of the IONPs in the setting process, delaying the precipitation of hydroxyapatite (HA), especially for contents greater than 10 wt %. The pH measurements were performed on the initial solution and on initial CPC paste with and without IONPs. The results showed that in both cases the pH is not affected by the presence of IONPs, whereas the values decreased in the paste due to the dissolution of phosphates in the liquid phase (Table 2).

Table 2: *pH measurements on liquid phase (Na_2HPO_4 solution) and initial pastes of CPCs.*

Sample	pH
Na_2HPO_4 solution	8.7
Na_2HPO_4 + 20% IONPs suspension	8.7
Initial paste	7.0
Initial paste + 20% IONPs	7.0

These results indicate that the initial local pH in the paste remained unchanged with the addition of 20 wt% IONPs, suggesting that the observed increase in setting time (t_i) is likely due to a slower precipitation kinetics provoked by the presence of nanoparticles in the matrix. The path of the setting reaction in these CPCs is determined by the solid constituents. TTCP and DCPA begin to dissolve, and dissolution proceeds until the composition of the solution reaches a constant value, which is represented by the intersection point between the TTCP and DCPA solubility curves at pH ≈ 8 [17]. When this point is reached, the dissolution of the reactants occurs as the precipitation of HA consumes Ca^{2+} and PO_4^{3-} ions from the aqueous solution. Thus, the reaction continues until one of the reactants runs out. Fukase *et al.* [17] reported that the formulation of TTCP and DCPA with water yields stoichiometric HA. However, subsequent investigations showed that only the first nuclei are composed by stoichiometric HA, while subsequent growth occurs in the form of calcium-deficient HA.

The analysis of setting times for the studied cement compositions allows us to conclude that an addition of 10 or 20 wt% of IONPs to the TTCP/DCPA mixture maintains setting kinetics like that of the cement without nanoparticles. This finding suggests that the incorporation of IONPs within the TTCP/DCPA matrix does not significantly alter the setting behavior of the cement. Such similarity in setting kinetics is essential for ensuring the practical viability and usefulness of the composite material in various biomedical applications, as it indicates that the addition of IONPs does not compromise the handling characteristics or setting time of the cement.

Hence, this study was aimed at conducting an in-depth characterization of samples containing 10 and 20 wt% of IONPs in comparison to the IONPs-free cement. By focusing on these specific compositions, we sought to gain a comprehensive understanding of how the incorporation of these amounts of IONPs influences the properties and performance of the cement matrix. This detailed analysis enables us to elucidate the effects of IONPs content on key parameters such as phase compositions, magnetic and antibacterial properties, and hyperthermia, providing valuable insights for the optimization of IONP-enhanced calcium phosphate cements for biomedical applications.

Figure 2 shows the XRD patterns of samples C, C10 and C20 after different incubation times at 100% relative humidity (RH). In every case, the conversion of the crystalline phases to hydroxyapatite is observed after 15 days, which is mainly evidenced by the presence of a broad peak at 32 ° 2Θ, and another peak of lower intensity at 26 ° 2Θ for the three compositions.

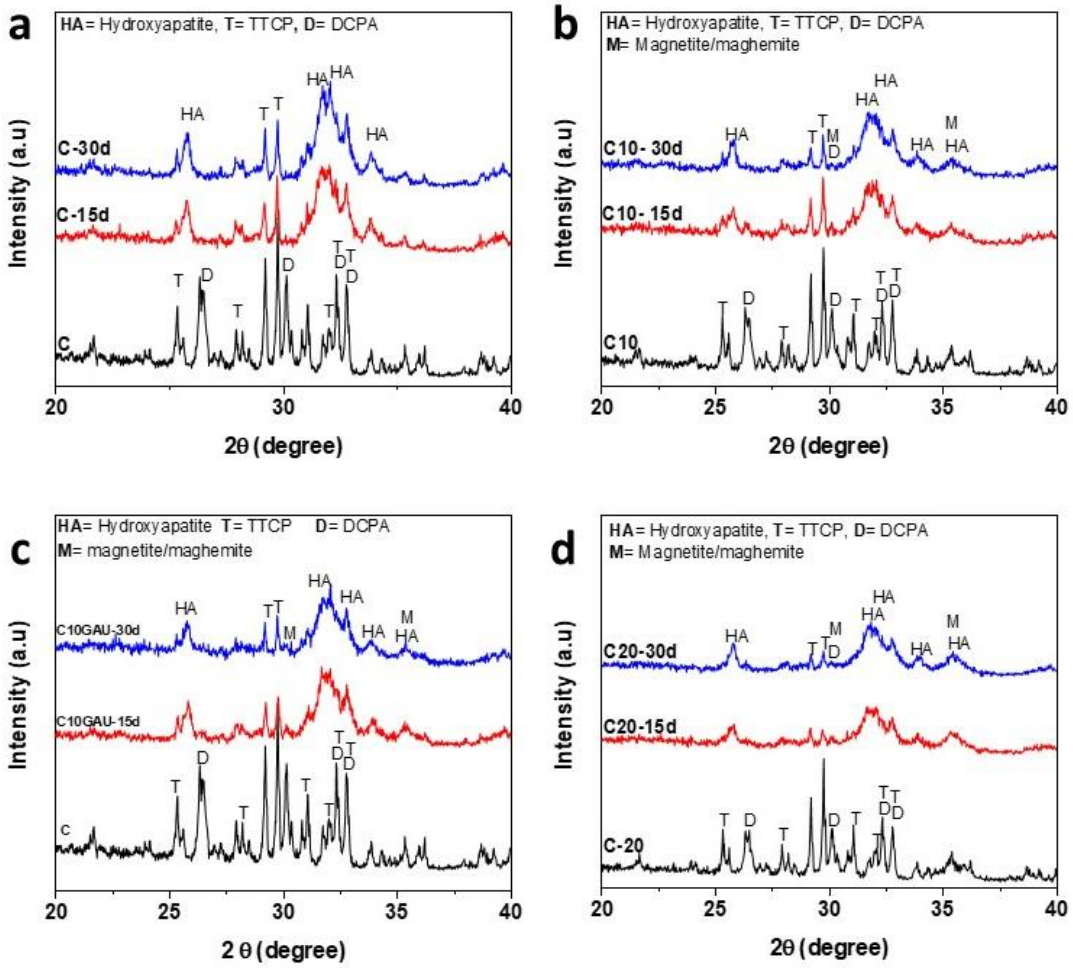

Figure 2: *XRD patterns of* ***a)*** *C,* ***b)*** *C10 and* ***c)*** *C10GAU,* ***d)*** *C20 samples set at different incubation times at 100% relative humidity (RH).*

According to the XRD patterns, the HA formation reaction takes place during the first 15 days of incubation at 100% RH, since there are no significant crystallographic changes at times longer than 15 days. However, after 60 days of incubation, the presence of residual phases of TTCP and DCPA in the cements is still observed. It should be noted that the main XRD peaks corresponding to the IONPs phases are superimposed with the peaks of the calcium phosphate phases.

The diffractograms of the CPCs with IONPs show a higher degree of conversion to HA (presumably non-stoichiometric), evidenced mainly by the decrease in the relative intensity of the TTCP peaks with the nanoparticle content. This can be explained considering that IONPs act as nucleation points for the formation of HA crystals. According to the setting parameters and the conversion of the starting reagents into HA, CPC formulations with 10 wt% IONPs are more suitable for biomedical applications [9,10].

It was chosen to incorporate 10 wt% of functionalized IONPs into the CPC matrix for comparative purposes because this composition demonstrates setting behavior like that of the additive-free cement. This selection allows for a meaningful comparison between the modified and unmodified formulations, providing insights into the effects of IONPs addition on various properties of the cement, including but not limited to setting kinetics, magnetic behavior, etc. The incorporation of 10 wt% IONPs was found to be effective in preserving the setting times (both initial and final) within clinically acceptable ranges, while ensuring a high degree of conversion to hydroxyapatite (HA). Additionally, this concentration of IONPs within hydrogels has been shown to be suitable for use as effectors in magnetic field-induced hyperthermia and for non-invasive imaging through MRI [18]. SEM and TEM images taken at two magnifications are shown in Figure 3 for both non-functionalized IONPs and functionalized IONPs (f-IONPs) samples. The

nanoparticles exhibit a uniform size distribution, with an average diameter of approximately 10 nm. Functionalization with silane and usnic acid does not significantly alter the quasi-spherical morphology or size of the IONPs. However, the f-IONP images reveal an increased nanoparticle aggregation, likely due to the silanization process.

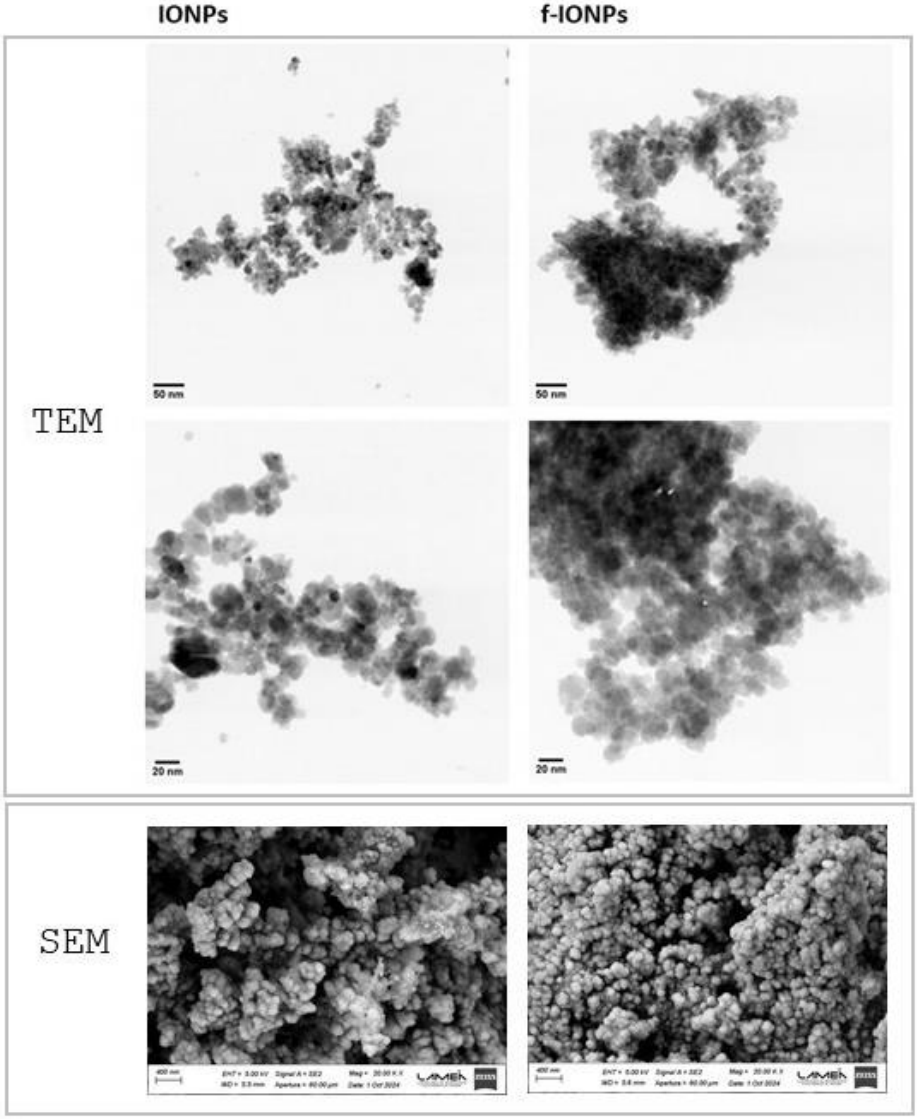

Figure 3. *TEM and SEM images for non-functionalized (IONPs) and functionalized nanoparticles (f-IONPs).*

Figure 4 shows SEM images of the fracture surface of the cements C, C10, C10GAU and C20 after 60 days of incubation at 100% HR. Moreover, EDS analysis to assess the dispersion of nanoparticles are included. The Ca/P mass ratio (measured on surface fracture) increases with the content of uncoated IONPs, which can be attributed to a reduced conversion of CPC to HA, except for the C10GAU sample. The presence of silanol groups may facilitate the formation of carbonated HA, as was reported by de Aza *et al.* [19-20]. The higher bioactivity of C10GAU is attributed to the concentration of silanol groups on the surface of these materials. The Ca/Fe mass ratio measured on the fracture surfaces reveals notable differences depending on whether the IONPs are functionalized or not. Uncoated IONPs serve as nucleation sites for HA crystallization, resulting in a microstructure characterized by well-defined, needle-like crystals. In contrast, functionalized IONPs induce a denser microstructure (C10GAU), marked by granular crystals and lower microporosity compared to other samples. The C10GAU sample exhibited a high degree of conversion to HA after 60 days of incubation, which can be attributed to the enhanced nucleation affinity of HA crystals on the surface of the siloxane network.

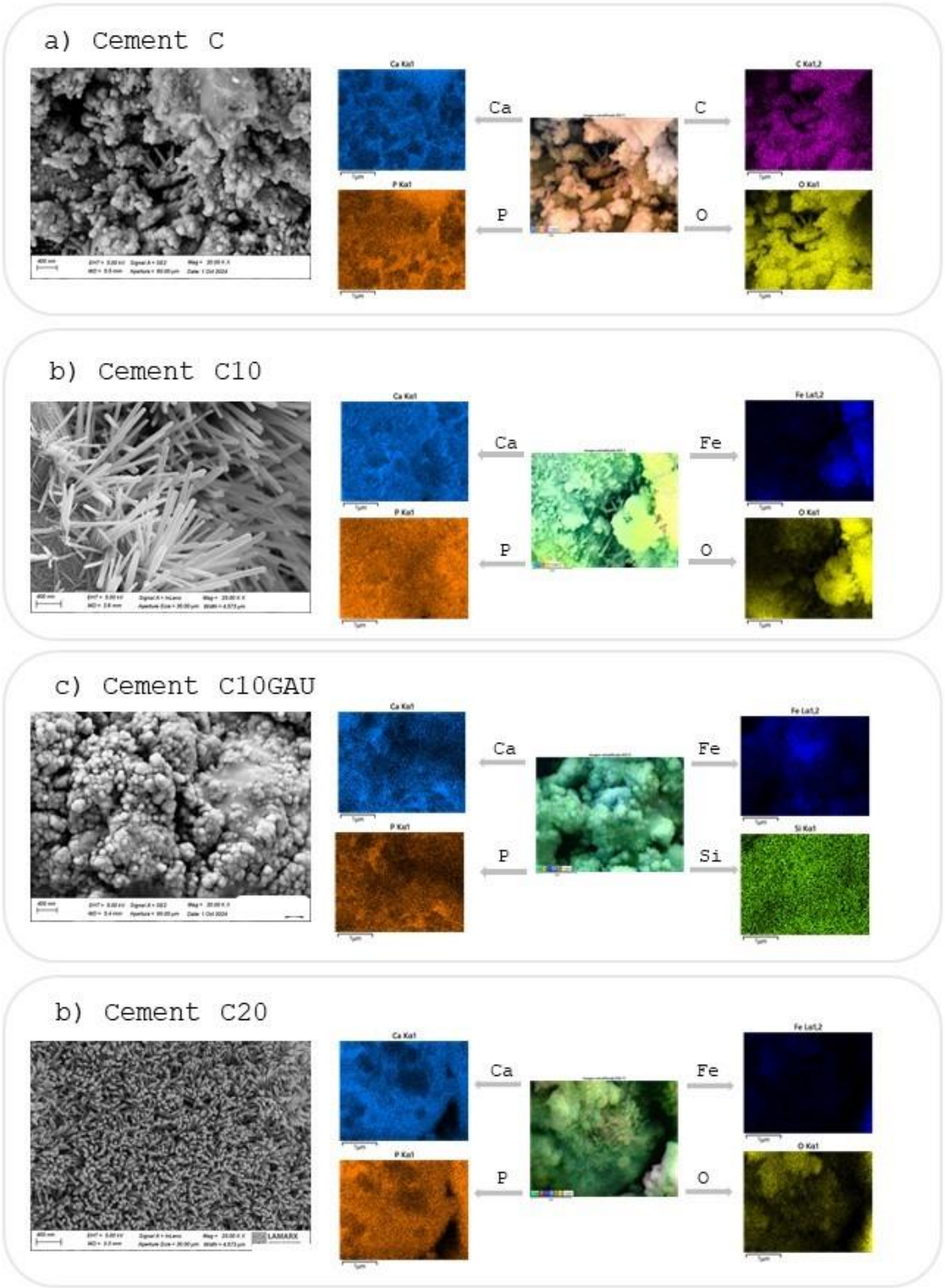

Figure 4: *SEM images of the fracture surface of the cements C, C10, C10GAU and C20 after 60 days of incubation at 100% HR and EDS mapping analysis.*

The acicular morphology of crystals observed for C10 and C20 is characteristic of the HA formation, as a product of the transformation of the starting reagents TTCP and DCPA. As the setting process progresses with incubation time in the humid chamber, the acicular crystals become more defined, indicating a greater proportion of crystallized HA in the cements [21]. The different morphology of C10 and C20 crystals compared to sample C is mainly due to the ability of the IONPs to facilitate the nucleation of the crystals. The microstructure of C20 appears more compact compared to C10, which can be attributed to the higher density of crystallization nuclei. The presence of Fe is seen specifically localized but distributed throughout the image, which demonstrates a very good distribution of the IONPs in the cement matrix. Furthermore, the estimated mass ratio Ca/Fe (for C10 and C20 respectively) are within the expected values according to the amount of IONPs nominally introduced into each material.

The C and C10GAU cements developed in this study were mechanically evaluated to compare their elastic modulus and hardness, focusing on the effect of functionalized IONPs. Table 3 summarizes the hardness (H), density, and reduced Young's modulus (Er) values for the tested samples.

Calcium phosphate cements (CPCs) are known to exhibit the mechanical behavior characteristic of brittle materials; however, their mechanical properties can be enhanced by incorporating strengthening agents. According to the literature, unreinforced CPCs typically display Er values around 3.8 GPa [22]. In this study, the Er value for the C10GAU sample was found to be 2.5 times higher than that of the C sample. This improvement in Er for C10GAU is attributed to the greater compaction observed in this sample, as evidenced by the microstructural analysis (SEM image) and supported by the density measurements.

Table 3: *Density, hardness (H), and reduced Young's modulus (Er) determined for the C and C10GAU samples.*

Sample	Density (g/cm^3)*	Hardness H (GPa)	Young's modulus reduced Er (GPa)
C	1.5 ± 0.1	0.039 ± 0.02	3.04 ± 0.6
C10GAU	1.7 ± 0.1	0.17 ± 0,08	7.77 ± 1.9

* *Determined by mass and geometrical measurements*

However, this increase in density is attributed to the enhanced compaction of the system and the higher density of the IONPs compared to the CPC matrix. Furthermore, the hardness values for the C10GAU sample were significantly higher than those of the C sample, with a more pronounced difference than observed in the Er values.

Samples C10 and C20 were magnetically characterized by determining the M vs H hysteresis loops measured after 0, 15 and 60 days of incubation at 100% RH. The curves recorded for both compositions are shown in Figure 5, obtaining at the maximum applied field (13 kOe) values of maximum magnetization *M*max=5.6 emu/g and *M*max=11.4 emu/g for IONPs aggregates of 10% and 20%, respectively.

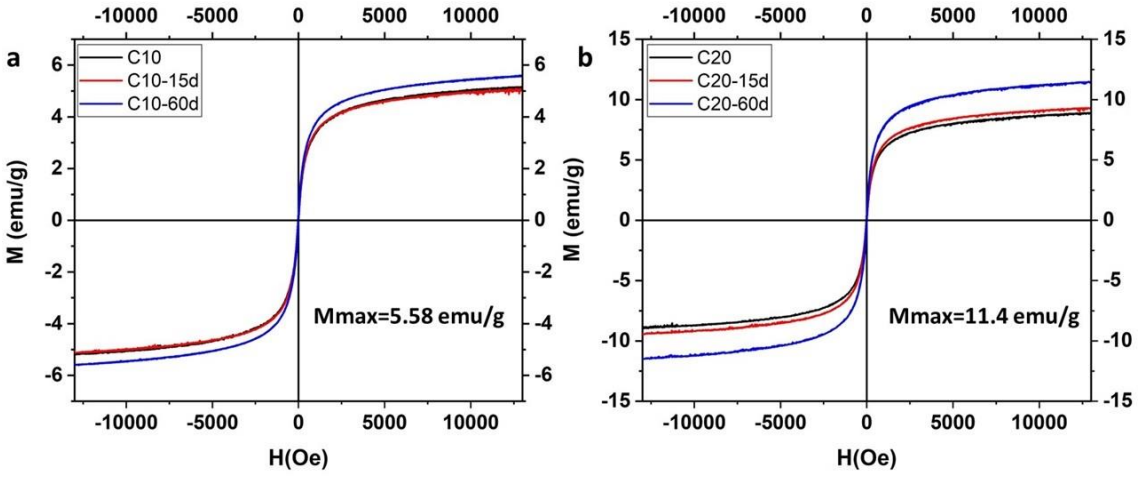

Figure 5: *Magnetic hysteresis loops M vs H of the cements after 0, 15 and 60 days of incubation at 100% RH:* ***a)*** *C10 and* ***b)*** *C20.*

The IONPs exhibit a magnetization of 62.7 emu/g, characteristic of pure nanoparticles [13]. In the C10 sample (cement with 10wt% IONPs), the magnetization is much lower, reflecting a significant dilution of the magnetic nanoparticles within the cement matrix. This reduction is expected due to the decreased concentration of IONPs, which affects the material's overall magnetic properties. The C20 sample (cement with 20wt% IONPs) exhibits a higher magnetization of 11.4 emu/g compared to C10. This increase is attributable to the higher concentration of magnetic nanoparticles in the mixture, although it remains considerably lower than that of the pure IONPs.

Table 4: *Maximum magnetization (Mmax) and coercivity (Oe) for CPC with IONPs in function of setting time (0,15 and 60 days of incubation time at 100%RH)*

	C10	**C10-15d**	**C10-60d**	**C20**	**C20-15d**	**C20-60d**
Mmax [emu/g]	5.1	5.1	5.6	8.5	9.4	11.4
Hc [Oe]	13.9	12.6	12.6	14.7	14.1	13.1

A quite stable magnetic behavior can be observed, with a slight increase in Mmax after setting for 60 days (Table 4). This result is compatible with a microstructural evolution towards smaller pores and less channels saturated with liquid, therefore modifying the CPC/IONPs mass ratio and increasing the magnetization (magnetic moment/mass ratio).
Coercivity values remain very low (around 13 Oe for both samples), which indicates that the magnetic nanoparticles retain their initial properties even after setting for 60 days. According to the measured magnetization values on the set cements as a function of time, it was determined that an addition of 10 wt% IONPs is enough to give rise to a significant magnetic signal useful for biomedical applications, in comparison with other reported works [5,11].
Furthermore, hyperthermia promoted by magnetic nanoparticles is potentially one of the most interesting applications of these materials [23]. When magnetic nanoparticles are placed in an alternating magnetic field which oscillates at frequencies of the order of hundreds of kHz, they can absorb power from the applied field due to the dephasing between the thermal relaxation of the particle magnetic moment and the field, generating heat and consequently increasing the temperature of the surrounding media. For example, when this technique is applied to tumor cells, they can heat up to 42-43°C and produce the cell apoptosis [7,23]. However, the effectiveness of this therapeutic method strongly depends on finding the optimal conditions for its application. A key parameter to evaluate the efficiency of magnetic hyperthermia is the specific power absorption (SPA), which represents, in an adiabatic system, the heat absorbed per unit of time (s) per gram of material. In this case the total mass includes both, the matrix and the IONPs and it is given by the following expression [24]:

$$SPA = \left(\frac{\Delta T}{\Delta t}\right) . c_p \qquad (1)$$

where $\Delta T/\Delta t$ is the rate of temperature change and Cp is the specific heat of the whole sample, mostly the matrix in which the magnetic nanoparticles are dispersed. Tests were carried out to determine the ability of the cements with a content of 10 and 20 wt% of naked IONPs to produce hyperthermia and the specific absorption rate of each material was calculated. The cement without added magnetic nanoparticles, sample C, was tested as a control material. Figure 7 shows the temperature increase profile corresponding to cements C, C10, C10GAU and C20 incubated for 60 days. Temperatures of all the compositions with IONPs gradually rise during the application of the magnetic field [25]. After 300 s, the magnetic field was removed, after which the temperature started to decrease exponentially. It is observed that the maximum temperature values reached are dependent on the IONPs content.
SPA values for each sample were calculated from the curves in Figure 6, where the values of $\Delta T/\Delta t$ were taken from the initial slope of each curve to reduce the effects of heat losses, which are proportional to the difference of temperature between the sample and the environment. The C_p value of the matrix was estimated as that of HA phase with an approximate porosity of 50%, (according to density measurements, not shown), and considering that the pores or channels are full of aqueous solution. Using the following specific heat values, $C_p(H_2O)$= 4.18 J (g °C)$^{-1}$ and C_p(HA)= 0.69 J (g °C)$^{-1}$ [26], an estimated value for the matrix C_p=2.435 J (g °C)$^{-1}$ was obtained. The cement C_p (C_p^{cement}) was calculated according to the following equation:

$$C_p^{cement} = x\ C_p^{IONPs} + (1\text{-}x)\ C_p^{matrix} \quad (2)$$

where "*x*" is the IONPs fraction in the cement. The used C_p^{IONPs} was 0.62 J (g ºC)$^{-1}$, assuming that IONPs are pure magnetite [27].

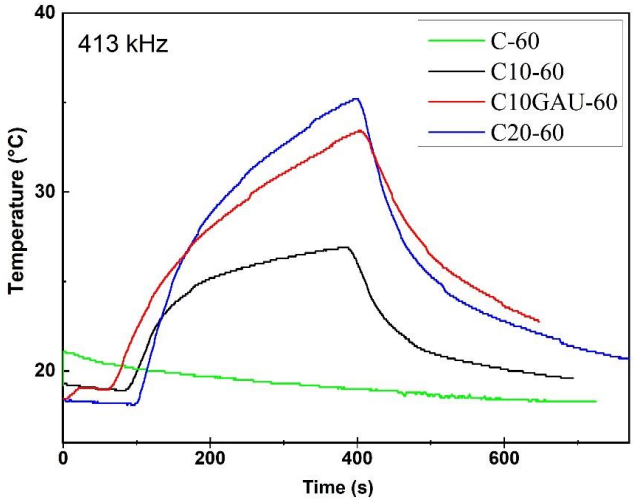

Figure 6: *Temperature as a function of time for different cements: An increase in temperature is recorded due to the application of a magnetic field for 300 seconds, followed by a decrease in temperature once the field is no longer applied.*

Table 5 summarizes the recorded $\Delta T/\Delta t$ values, as well as the calculated SPA values for each sample. In addition, the time values estimated to reach ΔT= 5ºC, assuming an adiabatic system, are presented. This temperature increment corresponds to a final temperature value of 42ºC, considering the initial temperature equal to the human body temperature (37 ºC).

Table 5: *Rate of temperature change, specific power absorption (SPA) and time required to reach ΔT= 5°C (t_{42}) in an adiabatic system.*

Sample	ΔT/Δt (°C/s)	SPA (W/g)	t_{42} (s)
C-60	----	----	----
C10-60	0.098	0.22	51
C10GAU-60	0.099	0.22	55
C20-60	0.143	0.30	35

The results revealed that sample C10 (both without C10 and with functionalization C10GAU) presents significantly lower values of $\Delta T/\Delta t$ and SPA than cements C20. This is an expected result considering that a higher content of IONPs produces a greater thermal effect, although this response is not linear, given that the dispersion and dipolar magnetic interactions between IONPs have a great influence on the hyperthermia behavior of the material [9]. It is noteworthy that, despite the similar maximum temperatures achieved by samples C10GAU and C20, the values of $\Delta T/\Delta t$ and t_{42} are significantly higher for C20 (Table 5). This suggests that the material containing 20wt% IONPs increases the temperature at a much faster rate compared to the sample with 10wt% functionalized IONPs. However, in the case of C10GAU, the magnetic nanoparticles are coated with an organic layer (siloxane and usnic acid) that can retain the generated heat more efficiently than uncoated IONPs, partially compensating for the registered maximum temperature values.

On the other hand, the functionalization of the cement C10GAU does not modify the hyperthermia behavior, which means that the nanoparticles can be efficiently functionalized and included in the cement matrix, as can be inferred by comparing the corresponding $\Delta T/\Delta t$ values in Table 5.

In all cases, the values t_{42} are greater than those usually reported for magnetic NPs in solution [28] and represent reasonable time values for using these materials in therapeutic applications. The power absorption of single domain magnetic particles from an applied alternating magnetic field occurs fundamentally through two different physical mechanisms which are related to the relaxation time of the magnetic moment: the Néel and Brown relaxations [29]. In our case, since these are IONPs dispersed in a solid matrix, Néel relaxation (activated thermal relaxation through an energy barrier) is the main phenomenon, although effects due to Brownian relaxation cannot be ruled out, due to the water content present in the cements. In this scenario, the saturation magnetization of the IONPs is not the only parameter that affects the heating properties, but other structural/physical parameters such as the size and distribution of the nanoparticles, the anisotropy, and the dipolar magnetic interactions between them, play a very important role [30, 31]. To elucidate the influence of all these effects, additional experiments must be performed to determine more rigorously the nature of the hyperthermia behavior observed in these composite materials.

Table 6 displays the inhibition zones observed following the exposure of four distinct bacterial strains to the tested samples. The results obtained for antibacterial activity indicated that both C and C10 did

not exert any activity (no inhibitions zones observed) against all the indicator pathogenic strains studied, indicating that neither the IONPs nor the cement matrix present antibacterial activity.

Table 6: *Antimicrobial activity for the different samples evaluated.*

		Growth inhibition zone (mm) ± SD			
		L.innocua	***S. aureus***	***E. coli***	***P. aeruginosa***
C	1	-	-	-	-
C10	2	-	-	-	-
C10GAU	3	13.3 ± 1.5	-	-	-
IONPs	4	-	-	-	-
C10	5	-	-	-	-
f-IONPs (I)	6	20.7 ± 1.0	-	-	17.7 ± 0.3
f-IONPs (II)	7	20.2 ± 0.6	-	-	15.5 ± 1.0
f-IONPs (III)	8	20.8 ± 0.8	-	-	17.5 ± 1.5
f-IONPs (IV)	9	22.3 ± 1.8	-	-	18.5 ± 1.0

Samples functionalized with usnic acid (f-IONPs I to IV) present antibacterial activity classified as extremely sensitive against *L. innocua*, and very sensitive for the *P. aeruginosa* strain; while for the *S. aureus* and *E. coli* strains, they do not present any type of antibacterial activity.

On the other hand, sample C10GAU showed antibacterial activity against *L. inoccua* classified as sensitive with 13.3 mm as inhibition zone diameter, while it did not exert any inhibitory effect against the rest of the strains. The result obtained for C10GAU can be explained considering the presence of usnic acid retained on the IONPs dispersed in the cement. This data is promising, considering that the concentration of IONPs in the cement is only equivalent to 10wt% of the material.

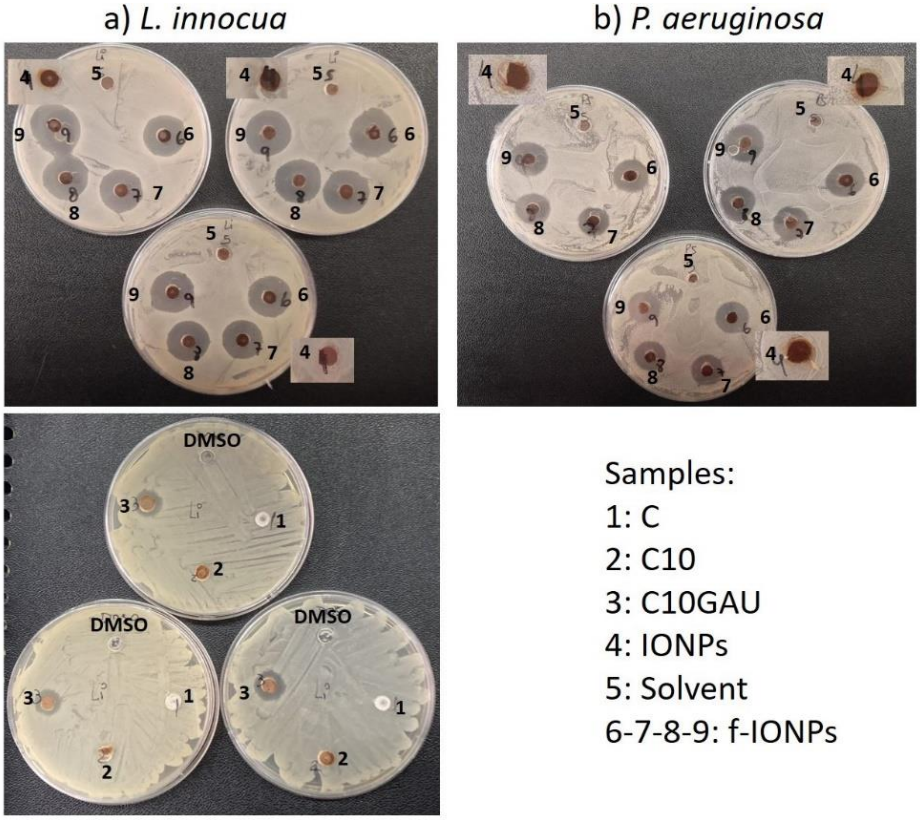

Figure 7: *Antibiogram of the samples evaluated against: a) L. innocua and b) P. aeruginosa strains by the Kirby-Bauer method.*

Figure 7.a) shows the growth inhibition zones caused by tested samples on *L. innocua* strain. It should be noted that in other studies in which the antibacterial effect of usnic acid was evaluated, it turned out to be effective against strains of *S. aureus* and *E. coli* but at higher concentrations than those used in this study [31,32]. This report confirmed that IONPs functionalized with usnic acid have antimicrobial

activity (very sensitive) for *P. aeruginosa* (Fig. 7.b), confirming that usnic acid concentration is a variable of utmost importance when evaluating the antibacterial behavior of the materials [33]. Beyond the findings of this study, it has been demonstrated that it is feasible to introduce antibacterial substances by functionalizing magnetic nanoparticles in the CPC.

Incorporating magnetic nanoparticles into CPCs offers a unique via for enhancing their functionalities, particularly in the field of magnetic hyperthermia therapy for cancer treatment.

Finally, magnetic nanoparticles, such as magnetite (Fe_3O_4) or maghemite (γ-Fe_2O_3), when dispersed within CPC matrices, exhibit magnetic properties that can be used for targeted drug delivery, hyperthermia treatment, and magnetic resonance imaging (MRI) contrast enhancement.

Moreover, the behavior of magnetic nanoparticles within the CPC matrix, influenced by factors such as nanoparticle size, shape, and concentration, as well as the characteristics of the surrounding biological environment, plays a critical role in determining the efficacy of these composite materials for biomedical applications.

4. CONCLUSIONS

New formulations of CPCs containing mechanochemically synthesized iron oxide nanoparticles (between 5-20 wt%) have been assayed as solid phase of bone cement, forming workable pastes and showing relatively low setting times, appropriate for a bone filler application. The crystallization of calcium phosphates into HA is strongly favored by the presence of IONPs, which act as nuclei for the growth of this phase crystals. The inclusion of IONPs in the cement matrix is not detrimental for their magnetic properties, obtaining magnetization and coercivity values suitable for the desired applications, particularly in hyperthermia treatments. The functionalization of IONPs with usnic acid gives CPC antimicrobial properties for the *L.innocua* strain. Increasing the concentration of this drug in the material could produce activity against other bacterial strains. The CPC/f-IONPs composite materials developed can be used as potential therapeutic bone cement, thanks to their magnetic properties, antibacterial capacity, and their ability to significantly increase the temperature when an external magnetic field is applied.

ACKNOWLEDGMENTS

The authors thank CONICET (PIP2863), UNMdP (15G/77) and FONCyT-Agencia (PICT2021-00797) for the funding given to this work.

REFERENCES

[1] W. Brown, Dental restorative cement pastes, United State Patent# 4518430 (1985) 1-14.

[2] H.E. Romeo, M.A. Fanovich, TTCP-DCPA Based Calcium Phosphate Cements Containing Hybrid Microparticles as Drug Carriers, Key Engineering Materials 396 (2009) 489-492.

[3] M. Ventura, Y. Sun, S. Cremers, P. Borm, Z.T. Birgani, P. Habibovic, A. Heerschap, P.M. van der Kraan, J.A. Jansen, X.F. Walboomers, A theranostic agent to enhance osteogenic and magnetic resonance imaging properties of calcium phosphate cements, Biomaterials 35 (2014) 2227-2233.

[4] M.R. DeBaun, J.C. Williams, C.G. Bennett, E.M. Pridgen, R.M. Tamurian, D.F. Amanatullah, Calcium phosphate cement and locked plate augmentation of distal femoral defects: A biomechanical analysis, Knee 26 (2019) 1020-1025. https://doi.org/10.1016/j.knee.2019.07.006.

[5] W. Zhong, L. Sun, T. Yu, C. Zhou, Preparation and characterization of calcium phosphate cement with enhanced tissue adhesion for bone defect repair, Ceramics International 47 (2021) 1712-1720. https://doi.org/10.1016/j.ceramint.2020.08.288.

[6] B. Liang, D. Zuo, K. Yu, X. Cai, B. Qiao, R. Deng, J. Yang, L. Chu, Z. Deng, Y. Zheng, G. Zuo, Multifunctional bone cement for synergistic magnetic hyperthermia ablation and chemotherapy of osteosarcoma, Materials Science and Engineering C 108 (2020). https://doi.org/10.1016/j.msec.2019.110460.

[7] E.A. Perigo, G. Hemery, O. Sandre, D. Ortega, E. Garaio, F. Plazaola, F.J. Teran, Fundamentals and advances in magnetic hyperthermia, Applied Physics Reviews 2 (2015).

[8] A. Pylostomou, O. Demir-Oguz, D. Loca, Calcium phosphate bone cements as local drug delivery systems for bone cancer treatment, Biomaterials Advances (2023) 213367.

[9] S. Zhao, K. Zhang, G. Li, Z. Zhang, X. Li, B. Cai, J. Li, Novel degradable super-paramagnetic bone cement with self-controlled hyperthermia ability, Materials & Design 218 (2022) 110676.

[10] Y. Xia, Y. Zhao, F. Zhang, B. Chen, X. Hu, M.D. Weir, A. Schneider, L. Jia, N. Gu, H.H.K. Xu, Iron oxide nanoparticles in liquid or powder form enhanced osteogenesis via stem cells on injectable calcium phosphate scaffold, Nanomedicine: Nanotechnology, Biology, and Medicine 21 (2019). https://doi.org/10.1016/j.nano.2019.102069.

[11] E.I. Ruskin, P.P. Coomar, P. Sikder, S.B. Bhaduri, Magnetic calcium phosphate cement for hyperthermia treatment of bone tumors, Materials 13 (2020) 3501.

[12] P.A. Calderón Bedoya, P.M. Botta, P.G. Bercoff, M.A. Fanovich, Magnetic iron oxides nanoparticles obtained by mechanochemical reactions from different solid precursors, Journal of Alloys and Compounds 860 (2021). https://doi.org/10.1016/j.jallcom.2020.157892.

[13] P.A.C. Bedoya, P.M. Botta, P.G. Bercoff, M.A. Fanovich, Influence of the milling materials on the mechanochemical synthesis of magnetic iron oxide nanoparticles, Journal of Alloys and Compounds 939 (2023) 168720. https://doi.org/10.1016/j.jallcom.2023.168720.

[14] H.E. Romeo, M.A. Fanovich, Synthesis of tetracalcium phosphate from mechanochemically activated reactants and assessment as a component of bone cements, Journal of Materials Science: Materials in Medicine 19 (2008) 2751-2760.

[15] B.D. Cullity, Elements of X-ray Diffraction, Addison-Wesley Publishing, 1956.

[16] M.C. Pellegrini, M.V. Alvarez, A.G. Ponce, N.M. Cugnata, F.G. De Piano, S.R. Fuselli, Anti-quorum sensing and antimicrobial activity of aromatic species from South America, Journal of Essential Oil Research 26 (2014) 458-465.

[17] Y. Fukase, E. Eanes, S. Takagp, L. Chow, W. Brown, Setting reactions and compressive strengths of calcium phosphate cements, Journal of Dental Research 69 (1990) 1852-1856.

[18] M. Ribeiro, M. Boudoukhani, E. Belmonte-Reche, N. Genicio, S. Sillankorva, J. Gallo, C. Rodríguez-Abreu, N. Moulai-Mostefa, M. Bañobre-López, Xanthan-Fe3O4 Nanoparticle Composite Hydrogels for Non-Invasive Magnetic Resonance Imaging and Magnetically Assisted Drug DeliveryACS Applied Nano Materials 2021 4, 7712-7729

[19] de Aza, P., et al, "Biocerámicas", in "Biomateriales" de Sastre, R., et al, Chapter 3, Faenza Editrice Iberica, España, 2004.

[20] Daniel Arcos, María Vallet-Regí, Sol–gel silica-based biomaterials and bone tissue regeneration, Acta Biomaterialia, 6, 8, 2010, 2874-2888, ISSN 1742-7061, https://doi.org/10.1016/j.actbio.2010.02.012.

[21] Z. Irbe, D. Loca, Soluble phosphate salts as setting aids for premixed calcium phosphate bone cement pastes, Ceramics International 47 (2021) 24012-24019.

[22] M. Nouri-Felekori, M. Khakbiz, N. Nezafati, J. Mohammadi, M. Baghaban Eslaminejad, N. Fani, Characterization and multiscale modeling of novel calcium phosphate composites containing hydroxyapatite whiskers and gelatin microspheres, Journal of Alloys and Compounds, 832, 2020, 154938, ISSN 0925-8388.

[23] D. Ortega, Q.A. Pankhurst, Magnetic hyperthermia, in: Nanoscience: Volume 1: Nanostructures through Chemistry, The Royal Society of Chemistry, 2012: pp. 60-88.

[24] K. Murase, Methods for Estimating Specific Loss Power in Magnetic Hyperthermia Revisited, Open Journal of Applied Sciences 6 (2016) 815-825.

[25] A.A. de Almeida, E. De Biasi, M.V. Mansilla, D.P. Valdés, H.E. Troiani, G. Urretavizcaya, T.E. Torres, L.M. Rodríguez, D.E. Fregenal, G.C. Bernardi, others, Magnetic hyperthermia experiments with magnetic nanoparticles in clarified butter oil and paraffin: a thermodynamic analysis, The Journal of Physical Chemistry C 124 (2020) 27709-27721.

[26] C. Caizer, Optimization study on specific loss power in superparamagnetic hyperthermia with magnetite nanoparticles for high efficiency in alternative cancer therapy, Nanomaterials 11 (2020) 40.

[27] T. Coelho, E. Nogueira, W. Weinand, W. Lima, A. Steimacher, A. Medina, M. Baesso, A. Bento, Thermal properties of natural nanostructured hydroxyapatite extracted from fish bone waste, Journal of Applied Physics 101 (2007).

[28] F. Grønvold, A. Sveen, Heat capacity and thermodynamic properties of synthetic magnetite (Fe3O4) from 300 to 1050 K. Ferrimagnetic transition and zero-point entropy, The Journal of Chemical Thermodynamics 6 (1974) 859-872.

[29] G.F. Goya, L. Asín, M.R. Ibarra, Cell death induced by AC magnetic fields and magnetic nanoparticles: current state and perspectives, International Journal of Hyperthermia 29 (2013) 810-818.

[30] D. Chang, M. Lim, J.A. Goos, R. Qiao, Y.Y. Ng, F.M. Mansfeld, M. Jackson, T.P. Davis, M. Kavallaris, Biologically targeted magnetic hyperthermia: Potential and limitations, Frontiers in Pharmacology 9 (2018) 831.

[31] M. Osaci, M. Cacciola, About the influence of the colloidal magnetic nanoparticles coating on the specific loss power in magnetic hyperthermia, Journal of Magnetism and Magnetic Materials 519 (2021) 167451.

[32] P. Chandika, F. Khan, S.-Y. Heo, Y.-M. Kim, M. Yi, W.-K. Jung, Enhanced wound-healing capability with inherent antimicrobial activities of usnic acid incorporated poly (ε-caprolactone)/decellularized extracellular matrix nanofibrous scaffold, Biomaterials Advances 140 (2022) 213046.

[33] M. Alavi, N. Karimi, Biosynthesis of Ag and Cu NPs by secondary metabolites of usnic acid and thymol with biological macromolecules aggregation and antibacterial activities against multi drug resistant (MDR) bacteria, International Journal of Biological Macromolecules 128 (2019) 893-901. https://doi.org/10.1016/j.ijbiomac.2019.01.177.